Original Research Article

Exploring 4-Aminonaphthalene Derivatives for Corrosion Inhibition through Density Functional Theory and Simulation on Iron Surface

Ayuba Abdullahi Muhammed[1], Fater Iorhuna[1,*], Thomas Aondofa Nyijime[2], Hussein Muhammadjamiu[1], Musa Sani[1]

[1]*Department of Pure and Industrial Chemistry, Bayero University Kano, Nigeria*
[2]*Department of Chemistry, Joseph Saawuan Tarka University Makurdi, Benue State, Nigeria*

Citation A. A. Muhammed, F. Iorhuna, T. A. Nyijime, H. Muhammadjamiu, M. Sani. Exploring 4-Aminnaphthalene Derivatives for Corrosion Inhibition through Density Functional Theory and Simulation on Iron Surface. *J. Eng. Ind. Res.* **2024**, 5(1):1-15.

https://doi.org/10.48309/JEIRES.2024.5.1

Article info:
Submitted: 2024-02-24
Revised: 2024-04-02
Accepted: 2024-04-21

Manuscript ID: JEIRES-2403-1113

Keywords:
Naphthalene; DFT; Corrosion; Iron-surface

ABSTRACT

The corrosion inhibition properties of naphthalene derivatives, including 4-amino-naphthalene-1-ol (4ANO), naphthalene-4-diamine (N4D), 4-amino-naphthalene-1-carboxylic acid (4ANC), 4-amino-2*H*-naphthalene-1-one (4AHN), and 4-amino-2*H*-naphthalene-1-thione (4AHT), were investigated on the Fe(111) surface. Computational methods, including density functional theory (DFT), were employed to evaluate various quantum parameters such as Fukui function, binding energy, and electronic properties including energy gap (ΔE), E_{HOMO}, E_{LUMO}, ionization energy (IE), electron affinity (AE), global hardness (η), softness (σ), number of electrons transferred (ΔN), global electrophilicity index (ω), electronegativity (χ), $\Delta E_{Back\text{-}donation}$, and electron-donating (ω^-) and accepting (ω^+) powers. The results revealed significant variations in the corrosion inhibition effectiveness among the studied naphthalene derivatives. 4ANO exhibited strong corrosion inhibition properties, attributed to its favourable interaction with the Fe(111) surface, as indicated by high binding energy and favourable quantum parameters. N4D and 4ANC also showed promising corrosion inhibition capabilities, although to a lesser extent compared to 4ANO. However, 4AHN and 4AHT displayed relatively weaker inhibition effects. Overall, this study provides valuable insights into the corrosion inhibition mechanisms of naphthalene derivatives on Fe(111) surfaces, offering guidance for the design and optimization of corrosion inhibitors for practical applications in metal protection and corrosion control.

Introduction

4-Aminonaphthalene is a molecule of significant interest in the field of corrosion inhibition due to its potential as an effective inhibitor for the presence of hetero atoms present. With a chemical structure comprising a naphthalene ring substituted with an amino group ($-NH_2$) at the 4-position, this compound possesses unique properties that make it a promising material for

***Corresponding Author: Fater Iorhun** (uyerfater22@gmail.com)*

mitigating corrosion [1]. The corrosion inhibition, particularly in metals like mild steel, is crucial in various industries to prevent structural degradation and ensure the longevity of metal components [2]. Mild steel is widely used in infrastructure, construction, and manufacturing due to its favourable mechanical properties, but it is susceptible to corrosion in corrosive environments [3-5]. The development of effective corrosion inhibitors is thus paramount to protect mild steel and extend its service life. Corrosion is a natural process that occurs when metals react with their environment, resulting in their deterioration or degradation. This process typically involves the formation of oxides or other compounds on the metal surface, which weakens its structure and can eventually lead to failure or loss of functionality [6,7]. Corrosion can be caused by various factors, including exposure to moisture, oxygen, acids, bases, salts, and pollutants in the environment. It is a widespread issue with significant economic and safety implications, as it can lead to the degradation of infrastructure, machinery, and equipment [8]. Preventive measures such as the use of corrosion-resistant materials, coatings, inhibitors, and proper maintenance practices are employed to mitigate corrosion and prolong the life-span of metal components though not accurate as scientist look for a more specific way to eliminate or reduce corrosion in our environment [9,10]. As such, DFT methods offer a powerful computational approach to study the interaction between moleculules of many organic structures on metals surfaces at the molecular level [11]. By employing DFT calculations, researchers can explore the adsorption behaviour of some molecules on the surface of mild steel and elucidate the underlying mechanisms of such molecules in inhibiting corrosion inhibition [12]. DFT simulations enable the prediction of crucial parameters such as adsorption energy, charge transfer, and molecular orientation, providing valuable insights into the effectiveness of molecules as a corrosion inhibitor [13]. By understanding the electronic structure and energetics of the molecule-metal interface, researchers can tailor the chemical properties of molecules to optimize its corrosion inhibition performance [4]. Through a combination of theoretical insights from DFT calculations and molecular dynamic simulation (MDS) validation, these efforts contribute to the advancement of materials science and the development of sustainable solutions for corrosion protection in various industrial applications [10]. Furthermore, DFT calculations can provide insights into the electronic structure of the inhibitor molecule and its influence on the corrosion process. By analysing frontier molecular orbitals, researchers can identify the sites of highest reactivity and understand the mechanism of inhibition at the molecular level [13]. In addition, simulation studies can explore the effect of environmental factors such as pH, temperature, and the presence of other chemical species on the corrosion inhibition efficiency, providing valuable guidance for practical applications [14]. This investigation is limited to the DFT study of derivatives of the four (4) 4-amino naphthalene on Fe(111) surface, namely 4ANO, N4D, 4ANC, 4AHN, and 4AHT. The molecules of the examined phytochemicals are shown in Scheme 1.

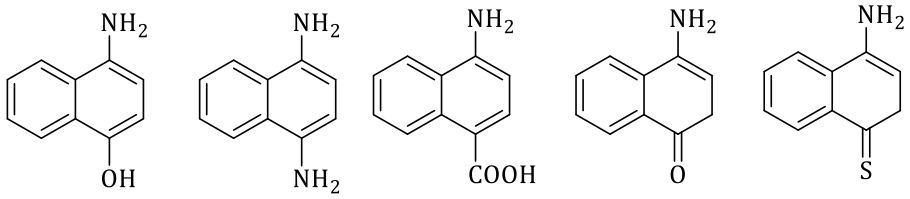

Scheme 1: Structure of naphthalene molecules

Experimental

Sketching of the studied molecules

ChemDraw Ultra 7.0.3 Cambridge Software was used to draw the molecules prior to determining their stable geometry [2].

Quantum chemical parameters calculations

The molecules of naphthalene were optimized using the DMol3 module in the BIOVIA Material Studio 8.0 software (Accelrys, Inc.). With the basis set to "double-numeric polarization" (DNP) in the aqueous phase model hence it is one technique for orienting nuclear spins in a solid is DNP. A microwave field is utilized to transfer the orientation of the electron spins to the nuclear spins on molecular structures and dynamics when the solid is slightly doped with unpaired electron spins. The parameters were calculated using the B3LYP function. The DFT quantum parameters that were derived in compliance with Koopman's extended theorem were computed using Equations 1-14 [15].

The ω^-, ω^+ powers and net electrophilicity ($\Delta\omega$) of the molecules was defined as shown in Equations (12-14), respectively:

$$IE = -E_{HOMO} \quad (1)$$

$$AE = -E_{LUMO} \quad (2)$$

$$\Delta E_g = E_{LUMO} - E_{HOMO} \quad (3)$$

$$\chi = \frac{IE+AE}{2} = -\frac{(E_{HOMO}+E_{LUMO})}{2} \quad (4)$$

$$\eta = \frac{IE-AE}{2} = \frac{(E_{LUMO}-E_{HOMO})}{2} \quad (5)$$

σ: $(eV)^{-1}$ $\sigma = \frac{1}{\eta} = -\frac{2}{E_{HOMO}-E_{LUMO}}$ (6)

$$\omega = \frac{\mu^2}{2\eta} = \frac{\chi^2}{2\eta} \quad (7)$$

μ: chemical potential (Debye) (8)

$\mu \approx -\frac{1}{2}(IE + AE) = \frac{1}{2}(E_{LUMO}+E_{HOMO})$

ε: nucleophilicity$(eV)^{-1}$ (9)

$$\varepsilon = \frac{1}{\omega}$$

ΔE_{b-d}: Energy of back donation (10)

$$\Delta E_{b-d} = -\frac{\eta}{4} = \frac{1}{8}(E_{HOMO} - E_{LUMO})$$

ΔN: Fraction of electron(s) transfer (11)

$$\Delta N = \frac{\chi Fe - \chi Inh}{2(\eta Fe + \eta Inh)}$$

$$\omega^- = \frac{(3IE+AE)^2}{16(IE-AE)} \quad (12)$$

$$\omega^+ = \frac{(IE+3AE)^2}{16(IE-AE)} \quad (13)$$

$$\Delta\omega^{\pm} = \omega^+ - (-\omega^-) = \omega^+ + \omega^- \quad (14)$$

Where, ηFe and ηInh are the absolute hardness of Fe and the inhibitor molecule, while χFe and χinh acted as Eigen values for the χ of Fe and the inhibitor molecule respectively. By assuming that for a metallic bulk IP=EA because they are softer than the neutral metallic atoms, a theoretical value for the electro-negativity of bulk iron was found as χFe = 7.0 eV and a η of iron surface as ηFe = 0eV [3,10,16,17]. Equation 15 is used to determine the second order

function of the molecules. Where f(+) is the f (+) and f- is the Fukui (-).

$$\Delta f(k) = f^{+}\text{-}f^{-} = f^{2} \quad \text{(Fukui function)} \quad (15)$$

MDS

Using a high stability quench adsorption approach on a surface of densely packed Fe(111) atoms, the studied pyrimidine derivatives were simulated. The FORCITE tool package, integrated inside the BIOVIA Materials Studio 8.0 software (Accelrys, Inc.), was utilized in the simulation process. The condensed-phase optimized molecular potentials for atomistic simulation studies (COMPASS) force field tool and the Smart algorithm approach were used in a simulation box measuring 17Å × 12Å × 28Å to execute computations in order to model a representative area of the surface. The Fe crystal was cleaved across by the (111) plane at a fractional depth of 3.0 Å. The bottom layers' form was constrained before the surfaces were optimized to avoid edge effects caused by the sizes of the molecules. A 5 × 4 supercell was then created by enlarging the surfaces. By maintaining the temperature at 350K, a compromise was achieved between a system with excessive kinetic energy, in which the molecule desorbs from the surface, and a system with inadequate kinetic energy, in which the molecule is unable to travel across the surface. With a simulation length of 5 ps and a time step of 1 fs, the temperature was set using the NVE (microcanonical) ensemble. It was envisaged that the process quench every 250 steps for a total of 5000 cycles in order to ascertain the statistical values of the energies on the surfaces of the Fe(111) crystal. Using FORCITE optimized geometries of the molecules and the Fe(111) surfaces, the lowest energy interactions of the molecules were discovered [3-4,10,14]. The adsorption and binding energies between the pyrimidine derivatives and the Fe(111) surface were calculated using Equations (12-18).

$$E_A = E_T - (E_I + E_S) \quad (16)$$

$$E_B = - E_A \quad (17)$$

Where, EB is the binding energy, ES is the energy of the iron surface, EA is the adsorption energy, EI is the inhibitor molecule's energy without the iron surface, and ET is the combined energy of the molecule and the iron surface [3,4,10,14].

Results and Discussion

The result presented in Figure 1 is the photo shoot of the studied 4-amino naphthalene; the pictorial result shows the highest occupied molecular orbital (HOMO) and the lowest unoccupied molecular orbital (LUMO) orbitals of the molecule where the HOMO and LUMO orbitals are located in the molecule. The result also presents the optimized molecule with the atomic orbitals been named. The electron density of the molecule is represented to show how the reaction of the molecule takes the entire molecule.

Fukui

Fukui's theory revolves around the notion of border molecular orbitals, which are a molecule's HOMO and LUMO. According to Fukui, the way electrons behave in these frontier orbitals determines a molecule's reactivity. Expanding on this notion, Fukui presented the idea of the Fukui function, which measures the change in electron density that occurs when an electron is added or removed from a specific atomic location inside a molecule [15-18]. The Fukui function is an important tool for understanding and predicting chemical reactivity since it shows how susceptible that atomic site is to chemical reactions through changes in electron density [19,20].

By offering a theoretical framework for comprehending and forecasting chemical reactivity at the molecular level, Fukui's function also transformed the discipline of theoretical chemistry [21]. The Fukui function is used to identify areas of a molecule in the context of a nucleophilic reaction where there is a strong tendency for electron density to raise with the addition of an electron [22]. Due to their electron abundance and deficiency, these regions correlate to locations within the molecule where

nucleophilic or electrophilic assaults are more favourable and can easily give or receive electrons to form new bonds, respectively [23]. As The Fukui function aids in predicting which molecular locations are most susceptible to nucleophilic assault in a similar manner, the reactivity of nucleophiles and the places they are most likely to target in a chemical reaction can be determined and understood by compounds through the analysis of the Fukui function. The Fukui function, in particular the nucleophilic Fukui function (f^-), offers important information about which atomic sites within molecules are most likely to be attacked by nucleophiles, and the electrophilic Fukui function (f^+) offers important information about which atomic sites within molecules are most likely to be attacked by electrophiles [24,25]. Among the Fukui values, the one with the highest value of Fukui is considered the most effective atom for the reaction activities for both nucleophilic and electrophilic [26]. In this study the result of Fukui function for the study molecules is obtained and presented in According to Table 1, the molecules studied in the table show greatness in the corrosion inhibition. The molecules 4ANO Fukui function was high at O12 and N11 for Fukui ($^+$) and Fukui ($^-$), N4D Fukui function was high at the Carbons C3, C6 and N11 for Fukui ($^+$) and Fukui($^-$), respectively, 4ACN Fukui functions occurs at O12 for Fukui ($^+$) and N11 for Fukui ($^-$) on the molecule 4AHT the Fukui functions were on C7 and S12 for Fukui ($^+$) and Fukui ($^-$) respectively. From the result according to Ayuba *et al.*, corrosion is favourable with molecules with heteroatom.

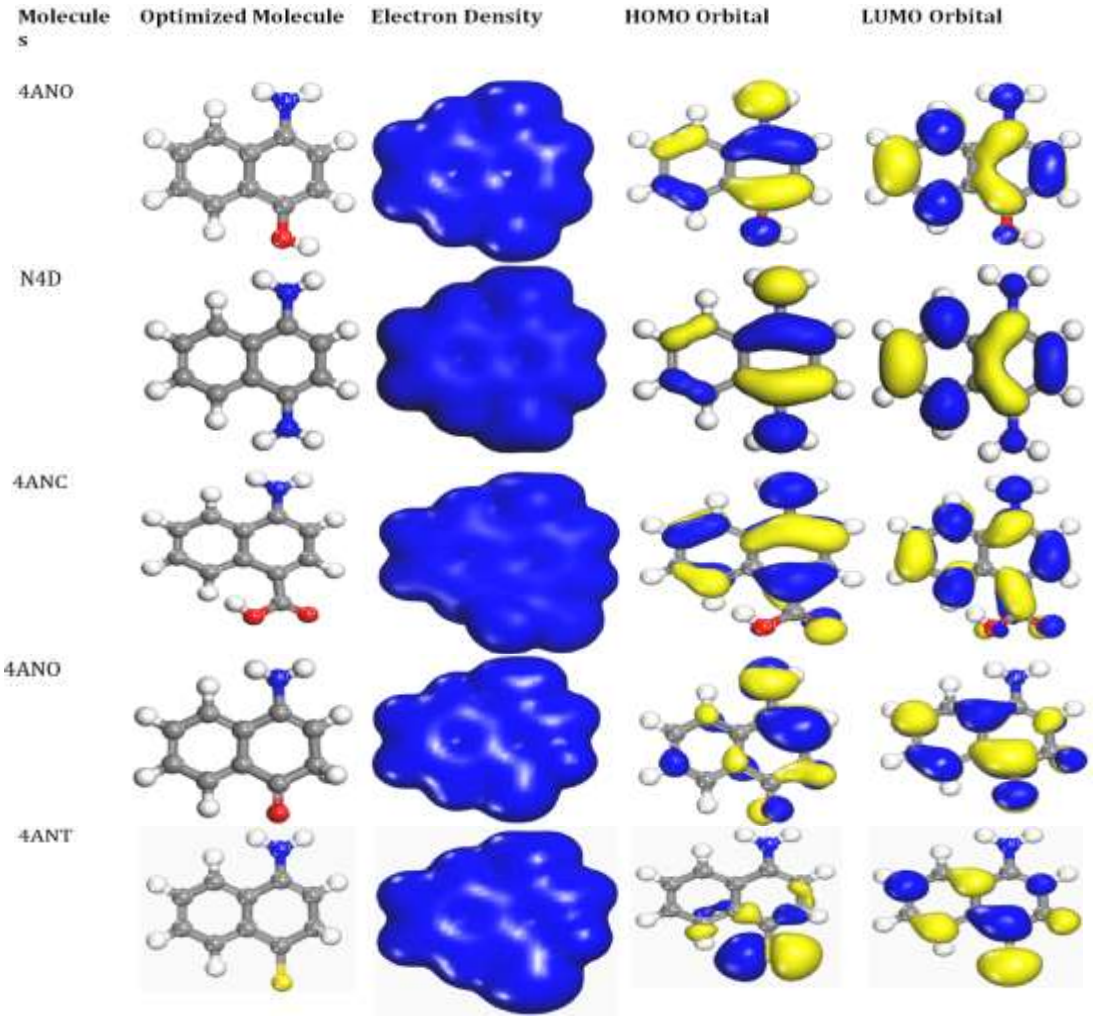

Figure 1: Optimized, electron density, homo, and lumo orbitals of the molecules 4ANO, N4D, 4ANC, 4ANO, and 4ANT

Table 1: The Fukui function of the studied molecules: 4ANO, N4D, 4ANC, 4AHN, 4AHT

F2	0.035	0.004	0.032	0.021	0.032	0.011	0.057	-0.005	-0.035	-0.026	-0.052	-
Fukui (-) 4AHT	0.046	0.04	0.021	0.006	0.012	0.029	0.031	0.028	0.071	0.045	0.077	-
Fukui (+) 4AHT	0.081	0.044	0.053	0.027	0.044	0.04	0.088	0.023	0.036	0.019	0.025	-
F2	0.054	-0.002	0.024	0.021	0.054	0.021	0.09	0.002	-0.106	-0.06	-0.137	0.058
Fukui (-) 4AHN	0.036	0.053	0.031	0.018	-0.004	0.023	0.014	0.024	0.145	0.079	0.161	0.081
Fukui (+) 4AHN	0.09	0.051	0.055	0.039	0.05	0.044	0.104	0.026	0.039	0.019	0.024	0.139
F2	-0.003	0.025	0.027	0.002	0.002	0.04	-0.044	0.026	-0.026	0.015	-0.054	-
Fukui (-) 4ACN	0.056	0.044	0.036	0.013	0.02	0.032	0.087	0.038	0.072	0.049	0.108	-
Fukui (+) 4ACN	0.053	0.069	0.063	0.015	0.022	0.072	0.043	0.064	0.046	0.064	0.054	-
F2	0.018	0.018	0.077	0.003	0.003	0.077	-0.019	-0.008	-0.008	-0.019	-0.072	-
Fukui (-) N4D	0.051	0.051	0.027	0.021	0.021	0.027	0.062	0.06	0.06	0.062	0.108	-
Fukui (+) N4D	0.069	0.069	0.104	0.024	0.024	0.104	0.043	0.052	0.052	0.043	0.036	
F2	0.054	-0.002	0.024	0.021	0.054	0.021	0.09	0.002	-0.106	-0.06	-0.137	0.058
Fukui (-) 4ANO	0.036	0.053	0.031	0.018	-0.004	0.023	0.014	0.024	0.145	0.079	0.161	0.081
Fukui (+) 4ANO	0.09	0.051	0.055	0.039	0.05	0.044	0.104	0.026	0.039	0.019	0.024	0.139
	C (1)	C (2)	C (3)	C (4)	C (5)	C (6)	C (7)	C (8)	C (9)	C (10)	N (11)	O (12)

	Fukui (+) 4ANO	Fukui (-) 4ANO	F2	Fukui (+) N4D	Fukui (-) N4D	F2	Fukui (+) 4ACN	Fukui (-) 4ACN	F2	Fukui (+) 4AHN	Fukui (-) 4AHN	F2	Fukui (+) 4AHT	Fukui (-) 4AHT	F2
N (12)	-	-	-	0.036	0.108	-0.072	-	-		-	-	-	-		-
C (12)	-	-	-	-	-	-	0.038	0.03	0.008	-	-	-	-	-	-
O (13)	-	-	-	-	-	-	0.079	0.097	-0.018	-	-	-	-		-
O (14)	-	-	-	-	-	-	0.041	0.05	-0.009	-	-	-	-	-	
S (12)	-	-	-	-	-		-	-	-	-	-	-	0.225	0.324	-0.099

Quantum chemical properties

Scientists examine a range of quantum chemical characteristics to get further insight into the dynamics of molecular interactions and energy transfer on the surface of metals. These characteristics provide important insights since they are derived from crucial molecular orbitals such as the lowest unoccupied molecular orbital (E_{LUMO}) and the highest occupied molecular orbital (E_{HOMO}). The ΔE, back donation energy (ΔE_{b-d}), dipole moment (μ), χ, η, σ, electron transfer percentage (ΔN), and ω are among the critical metrics that are being examined. Furthermore, essential elements of this analytical framework are the ω^- and ω^+.

ΔE, E_{HOMO}, and E_{LUMO}

The HOMO of the inhibitor molecule plays an important role in electron donation. An ω^- capacity that is greater is indicated by a higher energy HOMO, which enhances the inhibitor's ability to create a protective layer on the metal surface [20-23]. A stronger prevention of corrosion results from this enhanced adsorption strength. Furthermore, the energy of the HOMO influences the ability of the inhibitor molecules to form stable and protective barriers, highlighting its critical role in deciding how effective organic corrosion inhibitors are [24]. Higher energy HOMOs are often associated with increased inhibition because of better electron donation, increased adsorption, and increased barrier creation on the metal surface [25]. The 4ANC molecule has comparatively the highest value of E_{HOMO}, based on the findings of the study on Naphthalene derivatives. Consequently,4ANC >4AHN, 4ANO>N4D is the sequence in which the examined inhibitors' E_{HOMO} values fell, as provided in Table 2.

The inhibitor molecule's capacity to take in electrons from the metal surface or other species that donate electrons is determined by its LUMO energy [26]. Stronger ω^+ tendencies are implied by lower LUMO energy's, which promote interactions with the metal surface in the naphthalene derivatives studied, 4AHT has the lowest LUMO energy in the order of 4AHT< 4AHN< 4ANO< 4ANC< 4-N4D. By preventing access to corrosive agents, this electron acceptance can result in the creation of a stable complex or protective layer, which prevents corrosion [27].

Table 2: Quantum parameters of the molecules

Inhibitors	Molecules of naphthalene derivatives				
	4ANO	N4D	4ANC	4AHN	4AHT
E_{HOMO} (eV)	-4.128	-2.921	-4.629	-4.128	-4.065
E_{LUMO} (eV)	-1.938	-0.53	-1.886	-1.938	-2.572
ΔE (eV)	2.19	2.391	2.743	2.19	1.493
IE (eV)	4.128	2.921	4.629	4.128	4.065
AE (eV)	1.938	0.53	1.886	1.938	2.572
χ (eV)	3.033	1.726	3.258	3.033	3.319
η (eV)	1.095	1.196	1.372	1.095	0.747
σ $(eV)^{-1}$	0.913	0.836	0.729	0.913	1.339
ΔN	2.172	3.153	2.566	2.172	1.374
ω (eV)	5.036	1.779	7.277	5.036	4.11
ΔE_{b-d} (eV)	-0.274	-0.299	-0.343	-0.274	-0.187
ε $(eV)^{-1}$	0.199	0.562	0.137	0.199	0.243
ω^- (eV)	1.96	1.389	2.704	1.96	1.378
ω^+ (eV)	1.361	0.674	1.764	1.361	1.099
$\Delta\omega^{\pm}$(eV)	3.321	2.063	4.468	3.321	2.477

By modifying the metal's reactivity or passivating its surface, it also alters its electrical structure and prevents corrosion [23]. Reduced LUMO-HOMO gap facilitates electron transport to the inhibitor molecule from the metal surface [1,12,18-24]. The development of protective layers on the metal surface, which successfully prevent corrosion, depends on this electron transfer mechanism [2,15]. More effective electron transmission is made possible by a smaller ΔE, which improves corrosion prevention [28]. Because they are more likely to engage in redox processes, molecules with a smaller LUMO-HOMO gap might further increase their potency as corrosion inhibitors by offering more avenues for electron transfer and surface passivation [12,17].

IE and AE

The pivotal role of a molecule's ability to adhere to the metal surface cannot be overstated in corrosion inhibition. IE and AE dictate the distribution of charges within the molecule, thereby shaping its interaction with the metal surface [29]. Molecules exhibiting lower IE or higher AE tend to forge stronger bonds with the metal surface, thereby bolstering their adsorption and efficacy as inhibitors [2,4,11]. In contrast, heightened IE impedes electron donation, potentially obstructing the formation of protective layers. Lower IE or elevated AE may prompt swifter reactions with corrosive agents, fostering the creation of stable complexes or insoluble precipitates that deter corrosion [16-18]. In addition, molecules characterized by higher IE or lower AE are inclined to exhibit greater stability in corrosive environments, diminishing the risk of degradation and extending their lifespan as inhibitors. In the molecules studied in this study, IE is in the order of 4ANC> 4AHN, 4ANO> 4AHT> N4D and N4D> 4ANC> 4ANO> 4AHN> 4AHT respectively. [3,4,11,12-14].

η and σ

η and σ are concepts derived from conceptual DFT and are related to the reactivity of molecules. They can influence corrosion inhibition in the following ways: Adsorption, Electron Transfer, Chemical Reactivity, and Stability of the Inhibitor [30]. The η and σ of a molecule affect its ability to interact with the metal surface [10]. Molecules with higher hardness (η) have a greater resistance to

deformation of electron density, which may result in weaker interactions with the metal surface from the values of the η the values of the naphthalene derivatives presented in Table 2, 4ANC has the highest η. In contrast, 4AHT has the highest σ which is more prone to deformation and can form stronger interactions with the metal surface, enhancing their adsorption and corrosion inhibition properties on the Fe(111) surface [31].

ΔN

The computed electrons transferred (ΔN) from the naphthalene derivatives to iron metal are also listed in Table 2. The computed ΔN values are consistent with electron donation-based inhibitory efficiency discovered by Lukovit. Since each ΔN value was lower than 3.6, the N4D molecule had the greatest value. All of the compounds under investigation exhibit improved inhibitory efficacy as their ability to donate electrons to the metal surface rises. The electron donation capacity is arranged as follows, in increasing order of the acquired ΔN values: N4D > 4ANC > 4AHN > 4ANO > 4AHT [3,4,11,12-14]. Consequently, it is the inhibitor with the largest ΔN. These findings show a strong relationship between the factors listed and ΔN values.

The ω and χ

Parr developed the ω to quantify energy loss brought on by the greatest possible of electron flow between donor and acceptor entities. This index assesses the likelihood of chemical species to accept electrons, as stated in the Parr definition. Good electrophilic specie, on one hand, is characterized by a high value of μ and low ω, while on the other hand good nucleophilic specie is characterized by a lower value of μ and high ω. This novel reactivity index calculates the energy stabilization when the system absorbs an extra electrical charge ΔN from the surrounding environment. According to Sanderson's χ equalization concept, PMOs with high χ and low χ differential fast attain equalization and as a result, poor reactivity is anticipated, which in turn predicts low inhibition efficiency [3,4,11,12-14].

$\Delta EB_{ack\text{-}donation}$

The charge transferred to a molecule, followed by a back-donation from the molecule, is energetically preferred when:
$\eta > 0$ and $\Delta E_{back\text{-}donation} < 0$. Since there will be a contact with the same iron metal in this context, it is therefore conceivable to compare the stability of inhibitory molecules, and it is anticipated that the charge transfer will decrease as the hardness increases. Calculated $\Delta E_{back\text{-}donation}$ values for the inhibitors reported in Table 2 indicated that the best inhibitor PMS, is given preference for energy of back-donation [11,17]. This is in line with the other parameters observed in this work.

ω^- and ω^+ powers

The system's stabilizing energy, as it saturates with electrons from the environment, is quantified by the ω. Equation (12) defines the ω^-, while Equation (13) delineates the electron-receiving potency (ω^+). Consequently, a species with a higher ω^+ value exhibits superior charge-receiving ability, whereas one with a lower value excels in electron donation. To gauge the net electrophilicity ($\Delta\omega^+$), which elucidates the ω^+ potency relative to the ω^- capability, a comparison between ω^+ and ω^- values is proposed. Table 2 presents the computed net electrophilicity ($\Delta\omega^+$), ω^-, and electron-receiving (ω^+) capacities of the compounds. Corrosion inhibition involves molecules adhering to the metal surface, forming a protective layer that shields it from corrosive agents. The bond length between the inhibitor molecule and the metal surface plays a pivotal role in determining the strength of this adhesion [21]. Shorter bond lengths tend to foster stronger adhesion, thereby improving corrosion inhibition [28]. This enhanced adhesion may stem from heightened interactions between the inhibitor molecule and the metal surface, potentially facilitated by improved charge transfer or orbital overlap [12]. Overall, the impact of bond length on the corrosion inhibition of molecules on Fe metal hinges on factors like adsorption strength, electronic structure, stability, barrier formation, and steric effects [17] while shorter bond lengths typically promote stronger

interactions between the inhibitor molecule and the metal surface [1]. Table 3 indicates that the bond lengths connecting the majority of the heteroatoms are notably shorter compared to those linking the carbon atoms, with the exception observed at C7-S12 both before and after simulation on 4AHT molecule. This table is provided to assess the degree of interaction between the molecules and the simulated metal surface. The results indicate that most of the bonds decrease in size, while others increase, demonstrating significant interaction between the molecules and the metal surface [30-34]. single bond; this angle affects the molecule's conformation and how it interacts with the metal surface [22].

Table 3: The bond length of the molecules before and after simulation

Bond length of 4AHT	Before (A)	After	Bond length of 4ANC	Before	After	Bond length of N4D	Before	After
C1=C2	1.395	1.398	C1=C2	1.400	1.379	C1=C2	1.404	1.382
C2-C3	1.381	1.381	C2-C3	1.375	1.382	C2-C3	1.372	1.395
C3=C4	1.402	1.397	C3-C4	1.418	1.419	C3=C4	1.407	1.381
C4-C5	1.419	1.412	C4-C5	1.428	1.446	C4-C5	1.431	1.423
C5=C6	1.398	1.404	C5=C6	1.406	1.423	C5=C6	1.407	1.447
C4-C7	1.446	1.495	C1-C6	1.373	1.379	C6-C1	1.372	1.382
C7-C8	1.493	1.515	C4-C7	1.424	1.409	C4-C7	1.422	1.429
C8-C9	1.480	1.513	C7-C8	1.385	1.381	C7-C8	1.381	1.390
C9=C10	1.354	1.355	C8-C9	1.386	1.387	C8-C9	1.397	1.393
C10-C5	1.454	1.512	C9=CC10	1.386	1.392	C9=C10	1.381	1.390
C7=S12	1.700	3.305	C10-C5	1.428	1.437	C10-N11	1.380	1.407
C1-C6	1.356	1.393	C10-N11	1.363	1.409	C7-C12	1.380	1.408
C10-N11	1.378	1.363	C7-C12	1.465	1.492	C5-C10	1.422	1.430
			C12-O114	1.391	1.358			
			C12-O13	1.235	1.208			
Bond length of 4ANO	**Before**	**After**	**Bond length of 4AHN**	**Before**	**After**			
C1=C2	1.397	1.398	C1=C2	1.397	1.398			
C2-C3	1.387	1.387	C2-C3	1.391	1.390			
C3=C4	1.414	1.414	C3=C4	1.394	1.393			
C4-C5	1.435	1.435	C4-C5	1.404	1.406			
C5=C6	1.422	1.423	C5=C6	1.404	1.404			
C4-C7	1.418	1.417	C6-C1	1.391	1.391			
Bond length of 4ANO	**Before**	**After**	**Bond length of 4AHN**	**Before**	**After**			
C7-O12	1.388	1.387	C4-C7	1.493	1.495			
C7-C8	1.376	1.380	C7-C8	1.583	1.583			
C8-C9	1.377	1.390	C8-C9	1.500	1.505			
C9=C10	1.393	1.393	C9=C10	1.354	1.357			
C10-C5	1.428	1.427	C10-C5	1.514	1.517			
C10-N11	1.411	1.412	C10-N11	1.363	1.362			
			C7-O12	1.214	1.213			

The torsional angle of molecules affects their flexibility, adsorption, steric hindrance, and intermolecular interactions, all of which are important factors in determining how successful they are as corrosion inhibitors [13]. In Table 4, to confirm if the molecule interacts with the metal surface effectively, the torsional angle was investigated. The outcome demonstrates that all molecules of naphthalene interact with the metal surface, which is why the torsion angle values increase and decrease before and after inhibition [9].

Table 4: Torsion angle of naphthalene molecules

Torsion angle 4ANO	Before	After	Torsion angle 4AHN	Before	After
C6=C5-C10-N11	1.797	6.78	N11-C10-C5-C4	-173.882	171.434
N11-C10=C9-C8	179.028	176.479	N11-C10=C9-C8	-179.851	-178.242
C9-C8=C7-N12	-179.002	176.512	C9-C8-C7=O12	167.549	160.37
N12-C7-C4=C3	-1.869	6.863	O12-C7-C4=C5	172.726	165.98
Torsion angle 4ANC	**Before**	**After**	**Torsion angle 4AHT**	**Before**	**After**
O14-C12-C7-C4	-49.627	-46.004	C8-C7-C4=C3	-178.17	-178.178
O13-C12-C7=C8	-46.524	-41.886	S12=C7-C8-C9	-176.401	-176.409
N11-C10=C9-C8	179.414	-176.835	N11-C10-C9-C8	174.576	174.576
N11-C10-C5-C4	177.971	173.029	N11-C10-C5-C4	-179.083	-179.084
Torsion angle N4D	**Before**	**After**			
N11-C10-C9-C8	-177.819	-1177.82			
C9-C8-C7-O12	176.06	176.061			
O12-C7-C4=C5	-170.002	-170.003			

For a molecule to act as a corrosion inhibitor, it must adsorb onto the metal surface so as to create a protective layer [5,6]. The strength of the bonding between the inhibitor and the metal surface is indicated by the binding energy, that is, the amount of energy required to remove one mole of the inhibitor from the surface [19]. An inhibitor with a higher binding energy is likely to provide better protection to the metal surface [6]. From the molecules of naphthalene summarized in Table 5, 4ANO has the highest. This is because a greater amount of energy must be supplied to break the interaction between the inhibitor and the metal [4]. Likewise, it takes more time for the broken parts of the inhibitor to be removed from the

Table 5: Adsorption parameters for the interaction of naphthalene derivatives with the Fe(111) surface

Properties	Molecules				
	4ANO	N4D	4ANC	4AHN	4AHT
Energy of the Fe(111) (kcal/mol)	0.000	0.0000	0.0000	0.0000	0.0000
Adsorption energy (kcal/mol)	-80.058	-71.131	-80.551	-72.972	-75.111
Binding energy (kcal/mol)	80.058	71.131	42.66	72.972	75.111

metal surface so replacement of the inhibitor after being degraded is less likely [15]. The high values of the binding energies of the molecules indicated that, the molecules are capable of serving as anticorrosion agent on the iron surface. Though this inhibition is physisorption hence none of the binding energy values is more than 100kcal/mol as a threshold presented by

Ayuba *et al.* [14]. On the other hand, if the value exceeds 100 kcal/mol, the kinetic barriers to the inhibitor removal become very high and the inhibitor may become too stuck to the metal surface where chemisorption is needed for the inhibition mechanism [11]. Another important point to note is that binding energy is directly influenced by the electron density distribution around the inhibitor molecule, the cation in the metal that the inhibitor is interacting with, the local environment, temperature, presence of other reactants and the type of metal used [1-5]. Photo shoot of the molecules are depicted in Figure 2.

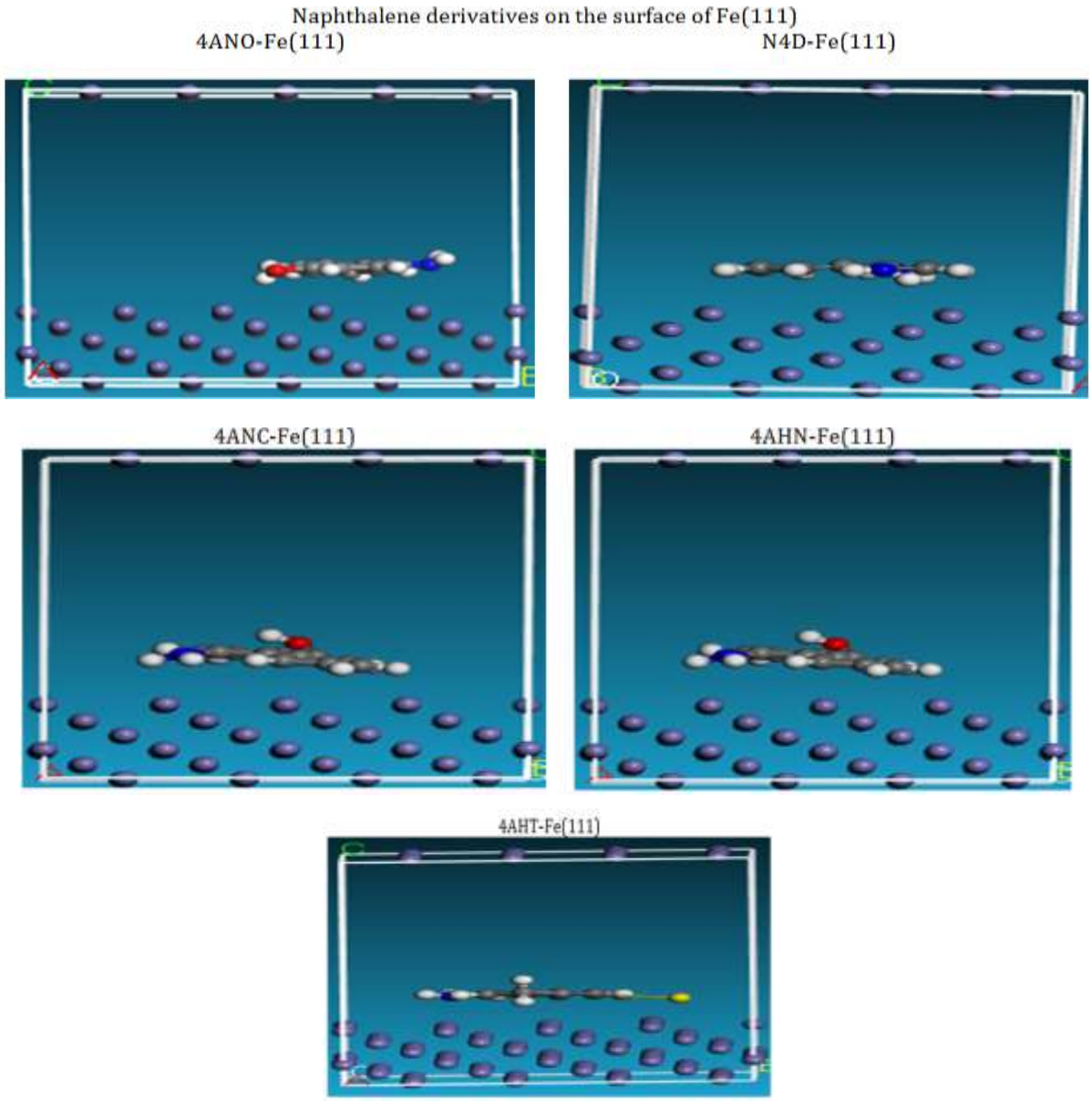

Figure 2: Naphthalene molecules on the surface of Fe(111) during simulation

Conclusion

To sum up, the investigation into the corrosion inhibition properties of naphthalene derivatives on the Fe(111) surface has provided valuable insights into their effectiveness as corrosion inhibitors. Through computational analysis employing DFT, we evaluated various quantum

parameters including Fukui function, binding energy, and electronic properties such as ΔE, IE, and χ. The results indicate that among the studied naphthalene derivatives, 4ANO exhibits the strongest corrosion inhibition properties, characterized by favourable interaction with the Fe(111) surface and high binding energy. N4D and 4ANC also demonstrate promising corrosion inhibition capabilities, albeit to a lesser extent compared to 4ANO. However, 4AHN and 4AHT exhibit relatively same level of inhibition but less compared to the 4ANC molecule of the naphthalene. These findings highlight the importance of molecular structure and electronic properties in determining the corrosion inhibition effectiveness of naphthalene derivatives. By elucidating the underlying mechanisms of corrosion inhibition, our study provides valuable guidance for the design and optimization of corrosion inhibitors for practical applications in metal protection and corrosion control. Moving forward, further experimental validation and testing of these naphthalene derivatives in real-world corrosion environments will be crucial to confirm their efficacy and explore their potential for industrial applications. In addition, future research could focus on optimizing the molecular structure of inhibitors to enhance their corrosion inhibition performance and broaden their applicability across different metal substrates and corrosive conditions.

ORCID

Ayuba Abdullahi Muhammed
https://orcid.org/0000-0002-2295-8282
Fater Iorhuna
https://orcid.org/0000-0002-1018-198X
Thomas Aondofa Nyijime
https://orcid.org/0000-0001-9537-1987
Hussein Muhammadjamiu
https://orcid.org/0009-0003-8235-5090
Musa Sani
https://orcid.org/0000-0001-5970-8167

Reference

[1]. J. Chen, X. Hu, J. Cui, Shikonin, vitamin K3 and vitamin K5 inhibit multiple glycolytic enzymes in MCF-7 cells, *Oncology Letters*, **2018**, *15*, 7423-7432. [Crossref], [Google Scholar], [Publisher]

[2]. H.A. AlMashhadani, K.A. Saleh, Electrochemical Deposition of Hydroxyapatite Co-Substituted By Sr/Mg Coating on Ti-6Al-4V ELI Dental Alloy Post-MAO as Anti-Corrosion, *Iraqi Journal of Science*, **2020**, 2751-2761. [Crossref], [Google Scholar], [Publisher]

[3]. L. Afandiyeva, V. Abbasov, L. Aliyeva, S. Ahmadbayova, E. Azizbeyli, H.M. El-Lateef Ahmed, Investigation of organic complexes of imidazolines based on synthetic oxy-and petroleum acids as corrosion inhibitors, *Iranian Journal of Chemistry and Chemical Engineering*, **2018**, *37*, 73-79. [Crossref], [Google Scholar], [Publisher]

[4]. H. Jafari, F. Mohsenifar, K. Sayin, Effect of alkyl chain length on adsorption behavior and corrosion inhibition of imidazoline inhibitors, *Iranian Journal of Chemistry and Chemical Engineering (IJCCE)*, **2018**, *37*, 85-103. [Crossref], [Google Scholar], [Publisher]

[5]. S. Elmi, M.M. Foroughi, M. Dehdab, M. Shahidi-Zandi, Computational evaluation of corrosion inhibition of four quinoline derivatives on carbon steel in aqueous phase, *Iranian Journal of Chemistry and Chemical Engineering (IJCCE)*, **2019**, *38*, 185-200. [Crossref], [Google Scholar], [Publisher]

[6]. L.T. Popoola, T.A. Aderibigbe, M.A. Lala, Mild steel corrosion inhibition in hydrochloric acid using cocoa pod husk-ficus exasperata: extract preparation optimization and characterization, *Iranian Journal of Chemistry and Chemical Engineering*, **2022**, *41*, 482-492. [Crossref], [Google Scholar], [Publisher]

[7]. R.M. Kubba, N.M. Al-Joborry, Theoretical study of a new oxazolidine-5-one derivative as a corrosion inhibitor for carbon steel surface, *Iraqi Journal of Science*, **2021**, 1396-1403. [Crossref], [Google Scholar], [Publisher]

[8]. K.A.K. Al-Rudaini, K.A.S. Al-Saadie, Milk thistle leaves aqueous extract as a new corrosion inhibitor for aluminum alloys in alkaline medium, *Iraqi Journal of Science*, **2021**, 363-372. [Crossref], [Google Scholar], [Publisher]

[9]. M.A. Mohammed, R.M. Kubba, Experimental Evaluation for the inhibition of carbon steel corrosion in salt and acid media by new derivative of quinolin-2-one, *Iraqi Journal of Science*, **2020**, 1861-1873. [Crossref], [Google Scholar], [Publisher]

[10]. S. Mammeri, N. Chafai, H. Harkat, R. Kerkour, S. Chafaa, Protection of steel against corrosion in acid medium using dihydropyrimidinone derivatives: experimental and DFT study, *Iranian Journal of Science and Technology, Transactions A: Science*, **2021**, *45*, 1607-1619. [Crossref], [Google Scholar], [Publisher]

[11]. T.V. Kumar, J. Makangara, C. Laxmikanth, N.S. Babu, Computational studies for inhibitory action of 2-mercapto-1-methylimidazole tautomers on steel using of density functional theory method (DFT), *International Journal of Computational and*

Theoretical Chemistry, **2016**, *4*, 1-6. [Crossref], [Google Scholar], [Publisher]
[12]. T. Esan, O. Oyeneyin, A. Olanipekun, N. Ipinloju, Corrosion inhibitive potentials of some amino acid derivatives of 1, 4-naphthoquinone–DFT calculations, *Advanced Journal of Chemistry Section A*, **2022**, *5*, 263. [Crossref], [Google Scholar], [Publisher]
[13]. R.M. Kubba, N.M. Al-Joborry, N.J. Al-lami, Theoretical and experimental studies for inhibition potentials of imidazolidine 4-one and oxazolidine 5-one derivatives for the corrosion of carbon steel in Sea Water, *Iraqi Journal of Science*, **2020**, 2776-2796. [Crossref], [Google Scholar], [Publisher]
[14]. Z. Yavari, M. Darijani, M. Dehdab, Comparative theoretical and experimental studies on corrosion inhibition of aluminum in acidic media by the antibiotics drugs, *Iranian Journal of Science and Technology, Transactions A: Science*, **2018**, *42*, 1957-1967. [Crossref], [Google Scholar], [Publisher]
[15]. N.M. Al-Joborry, R.M. Kubba, Theoretical and experimental study for corrosion inhibition of carbon steel in salty and acidic media by a new derivative of imidazolidine 4-one, *Iraqi Journal of Science*, **2020**, 1842-1860. [Crossref], [Google Scholar], [Publisher]
[16]. S. John, J. Joy, M. Prajila, A. Joseph, Electrochemical, quantum chemical, and molecular dynamics studies on the interaction of 4-amino-4*H*, 3, 5-di (methoxy)-1, 2, 4-triazole (ATD), BATD, and DBATD on copper metal in 1N H_2SO_4, *Materials and corrosion*, **2011**, *62*, 1031-1041. [Crossref], [Google Scholar], [Publisher]
[17]. M. Belghiti, S. Echihi, A. Dafali, Y. Karzazi, M. Bakasse, H. Elalaoui-Elabdallaoui, L. Olasunkanmi, E. Ebenso, M. Tabyaoui, Computational simulation and statistical analysis on the relationship between corrosion inhibition efficiency and molecular structure of some hydrazine derivatives in phosphoric acid on mild steel surface, *Applied surface science*, **2019**, *491*, 707-722. [Crossref], [Google Scholar], [Publisher]
[18]. M.M. Kadhim, L.A.A. Juber, A.S. Al-Janabi, Estimation of the efficiency of corrosion inhibition by Zn-dithiocarbamate complexes: a theoretical study, *Iraqi Journal of Science*, **2021**, 3323-3335. [Crossref], [Google Scholar], [Publisher]
[19]. M. Lu, D. Liu, C. Zhang, F. Sun, DFT calculations and experiments of oxidation resistance research on B, N, and Si multi-doped diamond films, *Applied Surface Science*, **2023**, *612*, 155865. [Crossref], [Google Scholar], [Publisher]
[20]. D. Glossman-Mitnik, Computational study of the chemical reactivity properties of the Rhodamine B molecule, *Procedia Computer Science*, **2013**, *18*, 816-825. [Crossref], [Google Scholar], [Publisher]
[21]. A. Nahlé, R. Salim, F. El Hajjaji, M. Aouad, M. Messali, E. Ech-Chihbi, B. Hammouti, M. Taleb, Novel triazole derivatives as ecological corrosion inhibitors for mild steel in 1.0 M HCl: experimental & theoretical approach, *RSC Advances*, **2021**, *11*, 4147-4162. [Crossref], [Google Scholar], [Publisher]
[22]. N.O. Eddy, P.O. Ameh, N.B. Essien, Experimental and computational chemistry studies on the inhibition of aluminium and mild steel in 0.1 M HCl by 3-nitrobenzoic acid, *Journal of Taibah University for Science*, **2018**, *12*, 545-556. [Crossref], [Google Scholar], [Publisher]
[23]. L. Guo, M. Zhu, J. Chang, R. Thomas, R. Zhang, P. Wang, X. Zheng, Y. Lin, R. Marzouki, Corrosion inhibition of N80 steel by newly synthesized imidazoline based ionic liquid in 15% HCl medium: experimental and theoretical investigations, *International Journal of Electrochemical Science*, **2021**, *16*, 211139. [Crossref], [Google Scholar], [Publisher]
[24]. H. Lgaz, S. Masroor, M. Chafiq, M. Damej, A. Brahmia, R. Salghi, M. Benmessaoud, I.H. Ali, M.M. Alghamdi, A. Chaouiki, Evaluation of 2-mercaptobenzimidazole derivatives as corrosion inhibitors for mild steel in hydrochloric acid, *Metals*, **2020**, *10*, 357. [Crossref], [Google Scholar], [Publisher]
[25]. F. Iorhuna, N.A. Thomas, S.M. Lawal, A Theoretical property of thiazepine and its derivatives on inhibition of aluminium Al (110) surface, *Algerian Journal of Engineering and Technology*, **2023**, *8*, 43-51. [Crossref], [Google Scholar], [Publisher]
[26]. G. Kılınççeker, M. Baş, F. Zarifi, K. Sayın, Experimental and Computational Investigation for (E)-2-hydroxy-5-(2-benzylidene) Aminobenzoic Acid Schiff Base as a Corrosion Inhibitor for Copper in Acidic Media, *Iranian Journal of Science and Technology, Transactions A: Science*, **2021**, *45*, 515-527. [Crossref], [Google Scholar], [Publisher]
[27]. T.A. Nyijime, H.F. Chahul, A. Ayuba, F. Iorhuna, Theoretical investigations on thiadiazole derivatives as corrosion inhibitors on mild steel, *Advanced Journal of Chemistry section A*, **2023**, *6*, 141-154. [Crossref], [Google Scholar], [Publisher]
[28]. N.U. Inbaraj, G.V. Prabhu, Corrosion inhibition properties of paracetamol based benzoxazine on HCS and Al surfaces in 1M HCl, *Progress in Organic Coatings*, **2018**, *115*, 27-40. [Crossref], [Google Scholar], [Publisher]
[29]. T.A. Nyijime, H.F. Chahul, P.I. Kutshak, A.M. Ayuba, F. Iorhuna, V. Okai, A. Hudu, Theoretical investigation of aluminum corrosion inhibition using chalcone derivatives, *Mediterranean Journal of Chemistry*, **2024**, *14*, 58-68. [Crossref], [Google Scholar], [Publisher]
[30]. K. Chinthapally, B.S. Blagg, B.L. Ashfeld, Syntheses of symmetrical and unsymmetrical lysobisphosphatidic acid derivatives, *The Journal of*

organic chemistry, **2022**, *87*, 10523-10530. [Crossref], [Google Scholar], [Publisher]
[31]. P. Muthukrishnan, B. Jeyaprabha, P. Prakash, Corrosion inhibition and adsorption behavior of Setaria verticillata leaf extract in 1M sulphuric acid, *Journal of Materials Engineering and Performance*, **2013**, *22*, 3792-3800. [Crossref], [Google Scholar], [Publisher]
[32]. A. Adegoke, G. Azeez, A. Lawal, M. Imran, Theoretical studies of 1, 2, 3-triazole and isoxazole-linked pyrazole hybrids as antibacterial agents: An approach of docking and density functional theory, *Advanced Journal of Chemistry, Section* B, **2021**, *3*,148. [Crossref], [Publisher]
[33]. A. Thakur, S. Kaya, A.S. Abousalem, S. Sharma, Richika Ganjoo, Humira Assad, Ashish Kumar, Computational and experimental studies on the corrosion inhibition performance of an aerial extract of Cnicus Benedictus weed on the acidic corrosion of mild steel, *Process Safety and Environmental Protection*, **2022** *161*, 801-818. [Crossref], [Google Scholar], [Publisher]
[34]. A.B. Adegoke, R.A. Adepoju, A.T.A. Khan, Molecular dynamic (MD) simulation and modeling the bio-molecular structure of human UDP glucose-6-dehydrogenase isoform 1 (hUGDH) related to prostate cancer, *Basrah Journal of Science*, **2020**, *38*, 448-466. [Crossref], [Google Scholar]